fcc-hcp phase transformation in Co nanoparticles induced by swift heavy-ion irradiation

D. J. Sprouster,* R. Giulian, C. S. Schnohr, L. L. Araujo, and P. Kluth
Department of Electronic Materials Engineering, Research School of Physics and Engineering, Australian National University, Canberra, Australian Capital Territory 0200, Australia

A. P. Byrne
Department of Physics, Faculty of Science, Australian National University, Canberra, Australian Capital Territory 0200, Australia

G. J. Foran and B. Johannessen
Australian Nuclear Science and Technology Organization, Menai, New South Wales 2234, Australia

M. C. Ridgway
Department of Electronic Materials Engineering, Research School of Physics and Engineering, Australian National University, Canberra, Australian Capital Territory 0200, Australia

(Received 28 November 2008; revised manuscript received 23 July 2009; published 30 September 2009)

We demonstrate a face-centered cubic (fcc) to hexagonally close-packed (hcp) phase transformation in spherical Co nanoparticles achieved via swift heavy-ion irradiation. Co nanoparticles of mean diameter 13.2 nm and fcc phase were first formed in amorphous SiO_2 by ion implantation and thermal annealing and then irradiated at room temperature with 9–185 MeV Au ions. The crystallographic phase was identified with x-ray absorption spectroscopy and electron diffraction and quantified, as functions of the irradiation energy and fluence, with the former. The transformation was complete at low fluence prior to any change in nanoparticle shape or size and was governed by electronic stopping. A direct-impact mechanism was identified with the transformation interaction cross-section correlated with that of a molten ion track in amorphous SiO_2. We suggest the shear stress resulting from the rapid thermal expansion about an ion track in amorphous SiO_2 was sufficient to initiate the fcc-to-hcp phase transformation in the Co nanoparticles.

DOI: 10.1103/PhysRevB.80.115438 PACS number(s): 61.46.Hk, 61.05.cj, 61.82.−d, 64.70.Nd

The enhanced magnetic[1] and optical[2] properties of metallic nanoparticles (NPs) have great potential for novel technological applications. Given both properties depend on particle size,[3] shape,[4,5] and structure,[4–6] an ability to control these parameters is a prerequisite for the efficient integration of NPs in advanced devices. Swift heavy-ion irradiation (SHII) is a novel means of modifying material properties, examples of which include (i) a spherical-to-rodlike shape transformation in metallic NPs (Refs. 7–15) embedded in amorphous SiO_2 (a-SiO_2) with the axis of elongation aligned parallel to the incident ion-beam direction, (ii) a monoclinic-to-tetragonal phase transformation in bulk oxides,[16] and (iii) a crystalline-to-amorphous phase transformation in bulk semiconductors.[17,18] During SHII, the incident ion-energy loss is dominated by electronic stopping through inelastic interactions with substrate electrons. Energy is subsequently transferred to the lattice by electron-phonon coupling and the resulting rapid increase in local temperature can yield a molten ion track of several nanometers in diameter.[19] Though a complete physical description of the shape transformation process for embedded metallic NPs is still lacking, NP melting followed by flow into the molten ion track has been suggested as a potential mechanism.[7,11,13,20,21]

Bulk Co can exist in either the ambient-stable hexagonally close-packed (hcp) phase or the face-centered-cubic (fcc) phase stable above 420 °C. The hcp-to-fcc transformation[22,23] is initiated via preformed cubic lamellae present well below the transformation temperature. While the hcp-to-fcc transformation is always complete, the reverse fcc-to-hcp transformation is incomplete with residual fcc structure observable after cooling to room temperature. A shear/dislocation-driven mechanism[22,24,25] can account for the incomplete transformation. SHII of bulk hcp Co results in the production of structural defects[26] but no change in crystallographic phase.

Co NPs can exist in either the hcp, fcc, or ε-Co phase, the relative stability of which depends on the route of formation,[4,5] host matrix,[27,28] and thermal history.[29,30] Of these three phases, hcp has the highest coercive field[5] and is thus the most obvious candidate for ultrahigh-density recording applications. For Co NPs formed in a-SiO_2 by ion-beam synthesis, only the hcp and fcc phases have been reported. The phase of such embedded Co NPs is governed by the Co concentration and annealing temperature. A residual fcc component is observable (at room temperature) only after annealing at temperatures of 800 °C (Refs. 29, 31, and 32) or higher. The formation of phase-pure fcc Co NPs stable at room temperature necessitates Co concentrations above 1 at. % and annealing temperatures of 900 °C or higher.[1,2,29,31] The stability of fcc-phase Co NPs at room temperature has been attributed to finite-size effects, specifically an enhanced surface tension.[30]

In this paper, we demonstrate the crystallographic phase of Co NPs formed by ion implantation and thermal annealing in a-SiO_2 can be readily controlled by SHII. We use x-ray absorption spectroscopy (XAS) and electron diffraction (ED) to monitor the irradiation-induced evolution of the fcc-to-hcp phase transformation as functions of irradiation energy and fluence and then consider the mechanism(s) potentially responsible for this change in phase. This methodology repre-

TABLE I. Computed parameters for Au ions in a-SiO_2 and Co as calculated by TRIM (Ref. 34) and the cross section for the fcc-to-hcp phase transformation calculated from fitting Eq. (1) to the experimental data.

Energy (MeV)	Range (μm)	a-SiO_2 S_e (keV/nm)	Co S_e (keV/nm)	a-SiO_2 S_n (keV/nm)	Co S_n (keV/nm)	σ (nm^2)
9	2	2.6	5.2	1.4	3.9	8.9(2.0)
27	6.3	4.8	9.4	0.7	2	31.0(2.5)
54	9.9	9	19.4	0.4	1.2	76.3(3.7)
89	13	12.7	29.8	0.3	0.9	89.2(4.5)
110	14.6	14.2	34.5	0.2	0.7	84.5(6.1)
185	19.2	17.6	45.1	0.2	0.5	92.5(5.8)

sents an effective means of controlling the crystallographic phase fractions to best suit specific technological applications.

Co ions were implanted into 2-μm-thick a-SiO_2 layers thermally grown on Si (100) substrates with all implants performed at liquid N_2 temperatures. Multiple energy (0.75, 1.00, and 1.40 MeV) and multiple fluence (4.4, 4.8, and $10.6\times10^{16}/cm^2$) implants were used to produce an essentially constant Co concentration of 3 at. % over depths of 0.75–1.40 μm. To induce Co precipitation and NP growth, samples were then annealed in flowing forming gas (5% H_2+95% N_2) for 1 h at a temperature of 1100 °C. The resulting volume-weighted mean NP diameter was 13.2 ± 3.7 nm as determined by both transmission electron microscopy (TEM) and small-angle x-ray scattering, the latter described elsewhere.[33] The samples were then irradiated at room temperature with Au ions at energies of 9, 27, 54, 89, 110, and 185 MeV, where the ion penetration depth was beyond that of the NP distribution. Au-ion fluences ranged from $10^{10}-2\times10^{13}/cm^2$. The electronic ($S_e$) and nuclear ($S_n$) stopping powers for Au ions in a-SiO_2 and Co, as calculated by TRIM,[34] are listed in Table I.

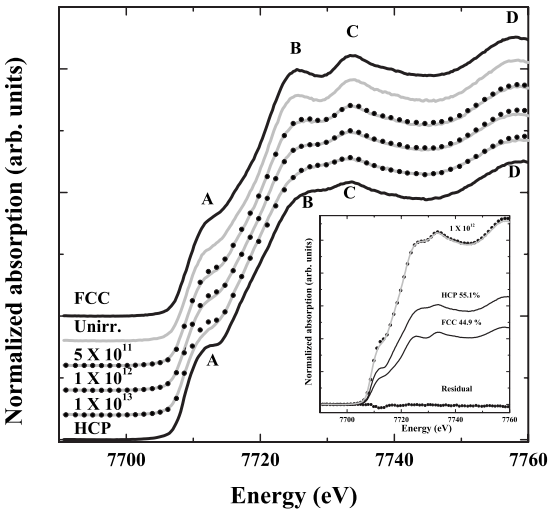

FIG. 1. XANES spectra for unirradiated bulk standards and NP samples irradiated at 185 MeV as a function of fluence ($/cm^2$). Solid circles represent the linear-combination fits to the experimental data with the inset showing the separate fcc and hcp contributions to the spectrum of the $1\times10^{12}/cm^2$ sample. Spectra have been vertically offset for clarity.

Fluorescence-mode XAS measurements were performed at beamline 20-B of the Photon Factory, Japan. Samples were measured at the Co *K* edge (7.709 keV) with the temperature maintained at 15 K to minimize thermal vibrations. X-ray absorption near-edge structure (XANES) spectra were recorded from 7.69–7.76 keV. After energy calibration and normalization, XANES spectra were fitted as a linear combination of hcp and fcc standards from 15 eV below to 50 eV above the edge. XANES spectra for the 185 MeV irradiations are shown in Fig. 1 as a function of fluence and the smooth transformation from fcc–to-hcp Co NPs is readily apparent. The XANES technique is well suited for the quantification of the phase fractions given the phase-dependent characteristic features (labeled A–D in Fig. 1) evident in the spectra of the two standards. These features result from multiple-scattering resonances of the 1*s* photoelectron in the continuum.[28,35] Our XANES spectrum for hcp Co agrees well with previous reports.[36–39] While multiple-scattering calculations[28,35] for fcc Co predict the amplitude of the B feature should exceed that of C, such a difference in relative amplitudes is not apparent in our XANES spectrum for fcc Co. However, the latter are consistent with XANES spectra for fcc Ni (Ref. 40) and thin fcc Co films grown on (111) Cu

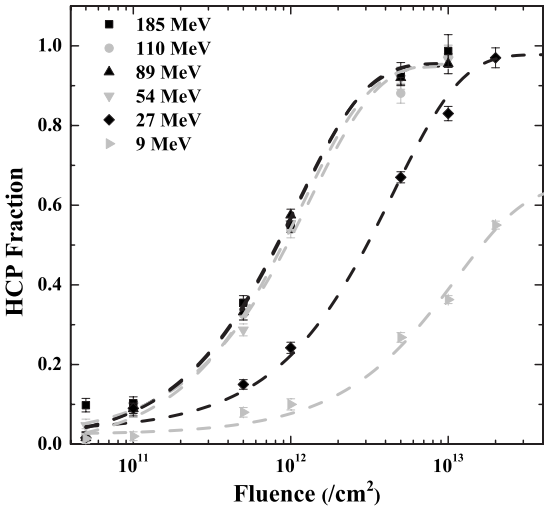

FIG. 2. hcp fraction from XANES in irradiated NP samples as a function of fluence. Fitted lines were derived from the Overlap model [Eq. (1)].

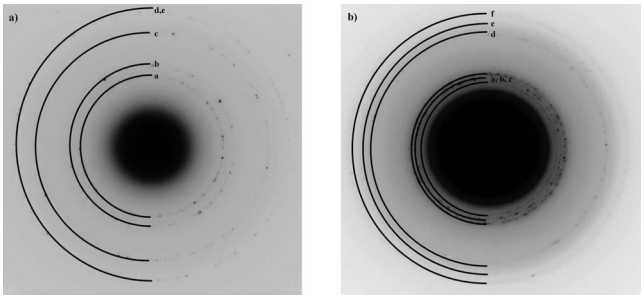

FIG. 3. Electron-diffraction patterns (a) before and (b) after irradiation with 89 MeV Au ions to a fluence of $2\times10^{13}/\mathrm{cm}^2$ (b). The calculated lattice spacings are listed in Table II.

substrates.[41] The most obvious difference in the XANES spectra of our two standards is the more pronounced dip between features B and C for the fcc phase. Nonetheless, fitting to quantify the hcp and fcc fractions was performed over the entire 7690–7760 energy range and thus included the additional phase-dependent features.

Figure 2 shows the hcp fraction as a function of fluence over the given range of irradiation energies. The fitted lines were generated with the Overlap model,[42]

$$\Delta C = C_S\left\{1-\sum_{k=0}^{n-1}\left[\frac{(\sigma\Phi)^k}{k!}\right]\exp(-\sigma\Phi)\right\}, \qquad (1)$$

where ΔC and C_s are the relative and total increases in hcp fraction, respectively, Φ is the irradiation fluence, and σ is the interaction cross section for the phase transformation. The best fit was achieved with $n=1$ and thus a direct-impact mechanism appears operative. For irradiation energies of 9–54 MeV, the rate of phase transformation clearly increases with energy demonstrating the process is governed by electronic stopping. Above 54 MeV, the rate saturates and is independent of irradiation energy. Irradiation of the bulk hcp and fcc Co standards of thickness 200 nm yielded no change in crystallographic phase.

Figures 3(a) and 3(b) show, respectively, TEM ED patterns (collected with a Phillips CM30 microscope operating at 300 kV) before and after the SHII of Co NPs at 89 MeV to a fluence of $2\times10^{13}/\mathrm{cm}^2$. The indexed lattice spacings (d) listed in Table II confirm the complete fcc-to-hcp phase transformation. Despite the latter, changes in the NP shape and size distributions were not apparent with TEM. High-resolution imaging also demonstrated the transformed hcp NPs were single crystalline like their unirradiated fcc counterparts. At greater fluences ($>2\times10^{13}/\mathrm{cm}^2$), the NP shape was progressively transformed from spherical-to-rodlike with a decrease in mean volume as a result of NP dissolution into the matrix, consistent with previous SHII studies of embedded Co NPs.[7,21] The fraction of Co atoms in an oxidized environment was also quantified using XANES with approximately 5% of the Co atoms in a Co_3O_4-like atomic configuration after the complete fcc-to-hcp phase transformation. Modeling of the XANES spectra demonstrated that the changes observable upon irradiation *were not* the result of Co atoms in an oxidized environment but *were* the result of the fcc-to-hcp phase transformation, the latter verified with TEM ED as discussed above.

Earlier observations of SHII-induced phase transformations in bulk metals[44] and oxides[16] differ from those reported herein. Benyagoub *et al.*,[16] for example, observed the transformation from a phase stable at ambient conditions to a high-temperature/high-pressure phase intuitively consistent with a rapid, post-thermal-spike quench. In contrast, Figs. 1 and 3 demonstrate the opposite for Co NPs where an irradiation-induced transformation from fcc- (stable at high-temperature/high-pressure in bulk material) to-hcp (stable at ambient conditions in bulk material) is apparent. The fcc-to-hcp transformation in bulk Co is martensitic and only proceeds when, in the presence of external forces, a critical shear energy is exceeded.[30] In free-standing Co NPs,[30] this barrier (~0.016 kJ/mol) can be overcome via the shear stress applied through mechanical grinding. In a-SiO_2 irradiated with swift heavy ions, large shear stresses result from the rapid thermal expansion of the cylindrical ion track. Using the Viscoelastic model,[45] we calculated the shear energy acting on a Co NP of 13.2 nm diameter increased from ~7 to ~63 kJ/mol over the SHII energy range of 9–185 MeV. The estimated values far exceed the critical shear energy for all irradiation energies. We thus suggest that shear stress in a-SiO_2 resulting from the formation of an ion track may well drive the fcc-to-hcp phase transformation in Co NPs.

We recently demonstrated the radial density distribution of an ion track resulting from SHII is consistent with a frozen-in acoustic pressure wave.[46] Figure 4 compares the interaction cross section for the irradiation-induced fcc-to-hcp phase transformation for Co NPs in a-SiO_2 [derived from Eq. (1)] with the irradiation-induced latent ion-track

TABLE II. Lattice spacing (d) determined from the electron-diffraction patterns of Fig. 3. Theoretical hcp and fcc spacings were calculated with (Ref. 43) $a=2.5$, $c=4.1$, and $a=3.5$ Å, respectively.

Sector	fcc (hkl)	$d_{(\mathrm{theory})}$ (Å)	Unirr. d (Å)	hcp (hkl)	$d_{(\mathrm{theory})}$ (Å)	2×10^{13} d (Å)
a	(111)	2.05	2.05(0.01)	(100)	2.17	2.17(0.01)
b	(200)	1.77	1.78(0.01)	(002)	2.03	2.03(0.01)
c	(220)	1.25	1.26(0.01)	(101)	1.92	1.91(0.01)
d	(311)	1.07	1.07(0.02)	(110)	1.25	1.25(0.02)
e	(222)	1.02	1.02(0.02)	(103)	1.15	1.16(0.02)
f				(112)	1.07	1.07(0.02)

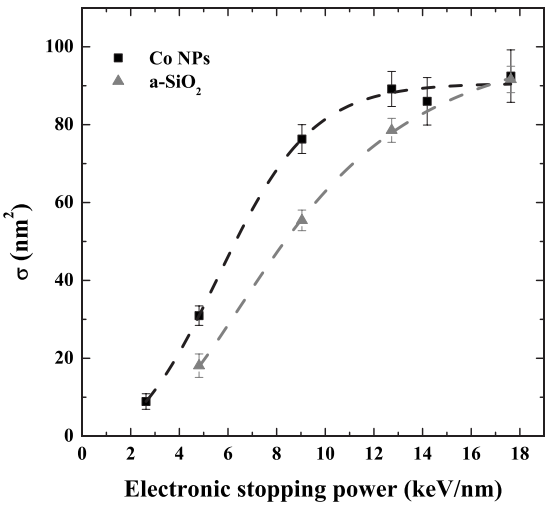

FIG. 4. Interaction cross section for the SHII-induced fcc-to-hcp phase transformation of Co NPs in a-SiO_2 and the latent ion-track cross section in a-SiO_2 (Refs. 46 and 47), both as a function of electronic stopping power.

cross section in a-SiO_2 (derived from small-angle x-ray scattering measurements and thermal-spike calculations[46,47]) as a function of electronic stopping power. The two are reasonably well correlated though, as noted above, the interaction cross section does saturate at high electronic stopping-power values. For irradiation energies of 89–185 MeV, our additional calculations of the energy-dependent and fluence-dependent macroscopic in-plane strain in a-SiO_2 yielded surprisingly similar values for the energy/fluence combinations required to complete the transformation. The saturation of the interaction cross section may thus be associated with attaining a given in-plane strain requirement.

We note that over the extent of the irradiation energies used in this paper, the electronic stopping power exceeded that necessary for molten ion-track formation in a-SiO_2 [$\sim$2 keV/nm (Ref. 48)]. Our model does not necessitate molten Co NPs and, in fact, thermal-spike calculations[49] predict the threshold electronic stopping power for a molten track in bulk Co is $\sim$30 keV/nm and as such melting is not anticipated at energies below 89 MeV.

In summary, we have shown that a simple adjustment of the swift heavy-ion irradiation energy and/or fluence is sufficient to tailor the crystallographic phase fractions of Co NPs in a-SiO_2. The irradiation-induced fcc-to-hcp transformation was the result of a direct-impact, electronic stopping-power-dependent process. We suggest the shear stress associated with the rapid thermal expansion about a molten ion track in a-SiO_2 was sufficient to initiate this technologically relevant phase transformation.

This work was financially supported by the Australian Synchrotron and the Australian Research Council. We thank M. Toulemonde, C. J. Glover, E. Frain, and I. McKerracher for helpful discussions.

*Email address: djs109@rsphysse.anu.edu.au

[1] M. Klimenkov, J. von Borany, W. Matz, D. Eckert, M. Wolf, and K. H. Muller, Appl. Phys. A: Mater. Sci. Process. **74**, 571 (2002).
[2] E. Cattaruzza, F. Gonella, G. Mattei, P. Mazzoldi, D. Gatteschi, C. Sangregorio, M. Falconieri, G. Salvetti, and G. Battaglin, Appl. Phys. Lett. **73**, 1176 (1998).
[3] C. Clavero, B. Sepulveda, G. Armelles, Z. Konstantinovic, M. G. del Muro, A. Labarta, and X. Batlle, J. Appl. Phys. **100**, 074320 (2006).
[4] Y. J. Song, H. Modrow, L. L. Henry, C. K. Saw, E. E. Doomes, V. Palshin, J. Hormes, and C. Kumar, Chem. Mater. **18**, 2817 (2006).
[5] S. Sun and C. B. Murray, J. Appl. Phys. **85**, 4325 (1999).
[6] V. F. Puntes, K. M. Krishnan, and P. Alivisatos, Appl. Phys. Lett. **78**, 2187 (2001).
[7] C. D'Orleans, J. P. Stoquert, C. Estournes, C. Cerruti, J. J. Grob, J. L. Guille, F. Haas, D. Muller, and M. Richard-Plouet, Phys. Rev. B **67**, 220101(R) (2003).
[8] A. Oliver, J. A. Reyes-Esqueda, J. C. Cheang-Wong, C. E. Roman-Velazquez, A. Crespo-Sosa, L. Rodriguez-Fernandez, J. A. Seman, and C. Noguez, Phys. Rev. B **74**, 245425 (2006).
[9] J. J. Penninkhof, T. van Dillen, S. Roorda, C. Graf, A. van Blaaderen, A. M. Vredenberg, and A. Polman, Nucl. Instrum. Methods Phys. Res. B **242**, 523 (2006).
[10] S. Roorda, T. van Dillen, A. Polman, C. Graf, A. van Blaaderen, and B. J. Kooi, Adv. Mater. (Weinheim, Ger.) **16**, 235 (2004).
[11] M. C. Ridgway, P. Kluth, R. Giulian, D. J. Sprouster, L. L. Araujo, C. S. Schnohr, D. J. Llewellyn, A. P. Byrne, G. J. Foran, and D. J. Cookson, Nucl. Instrum. Methods Phys. Res. B **267**, 931 (2008).
[12] R. Giulian, P. Kluth, L. L. Araujo, D. J. Sprouster, A. P. Byrne, D. J. Cookson, and M. C. Ridgway, Phys. Rev. B **78**, 125413 (2008).
[13] K. Awazu, X. Wang, M. Fujimaki, J. Tominaga, H. Aiba, Y. Ohki, and T. Komatsubara, Phys. Rev. B **78**, 054102 (2008).
[14] Y. K. Mishra, F. Singh, D. K. Avasthi, J. C. Pivin, D. Malinovska, and E. Pippel, Appl. Phys. Lett. **91**, 063103 (2007).
[15] P. Kluth, R. Giulian, D. J. Sprouster, C. S. Schnohr, A. P. Byrne, D. J. Cookson, and M. C. Ridgway, Appl. Phys. Lett. **94**, 113107 (2009).
[16] A. Benyagoub, Phys. Rev. B **72**, 094114 (2005).
[17] W. Wesch, A. Kamarou, and E. Wendler, Nucl. Instrum. Methods Phys. Res. B **225**, 111 (2004).
[18] C. S. Schnohr, P. Kluth, A. P. Byrne, G. J. Foran, and M. C. Ridgway, Phys. Rev. B **77**, 073204 (2008).
[19] M. Toulemonde, C. Dufour, and E. Paumier, Phys. Rev. B **46**, 14362 (1992).
[20] S. Klaumunzer, Nucl. Instrum. Methods Phys. Res. B **244**, 1 (2006).
[21] D. J. Sprouster, R. Giulian, C. S. Schnohr, L. L. Araujo, P. Kluth, D. J. Llewellyn, A. P. Byrne, G. J. Foran, D. J. Cookson, and M. C. Ridgway (unpublished).
[22] P. Toledano, G. Krexner, M. Prem, H. P. Weber, and V. P. Dmi-

triev, Phys. Rev. B **64**, 144104 (2001).
[23] C. S. Yoo, P. Soderlind, and H. Cynn, J. Phys.: Condens. Matter **10**, L311 (1998).
[24] F. Frey and H. Boysen, Acta Crystallogr., Sect. A: Cryst. Phys., Diffr., Theor. Gen. Crystallogr. **37**, 819 (1981).
[25] B. Strauss, F. Frey, W. Petry, J. Trampenau, K. Nicolaus, S. M. Shapiro, and J. Bossy, Phys. Rev. B **54**, 6035 (1996).
[26] A. Dunlop and D. Lesueur, Radiat. Eff. Defects Solids **126**, 123 (1993).
[27] J. C. Cezar, H. C. N. Tolentino, and M. Knobel, Phys. Rev. B **68**, 054404 (2003).
[28] G. L. Zhang, Z. Y. Wu, A. G. Li, Y. S. Wang, J. Zhang, M. I. Abbas, R. Hu, X. B. Ni, Y. P. Tong, and Y. K. Hwu, Phys. Rev. B **69**, 115405 (2004).
[29] L. G. Jacobsohn, M. E. Hawley, D. W. Cooke, M. F. Hundley, J. D. Thompson, R. K. Schulze, and M. Nastasi, J. Appl. Phys. **96**, 4444 (2004).
[30] X. Q. Zhao, S. Veintemillas-Verdaguer, O. Bomati-Miguel, M. P. Morales, and H. B. Xu, Phys. Rev. B **71**, 024106 (2005).
[31] G. Mattei, C. Maurizio, C. D. Fernandez, P. Mazzoldi, G. Battaglin, P. Canton, E. Cattaruzza, and C. Scian, Nucl. Instrum. Methods Phys. Res. B **250**, 206 (2006).
[32] C. Maurizio, G. Mattei, P. Canton, E. Cattaruzza, C. D. Fernandez, P. Mazzoldi, F. D'Acapito, G. Battaglin, C. Scian, and A. Vomiero, Mater. Sci. Eng., C **27**, 193 (2007).
[33] D. Sprouster, R. Giulian, L. L. Araujo, P. Kluth, B. Johannessen, D. J. Cookson, G. J. Foran, and M. C. Ridgway (unpublished).
[34] J. F. Ziegler, J. P. Beirsack, and U. Littmark, *The Stopping and Range of Ions in Matter* (Pergamon, New York, 1985).
[35] J. Hormes, H. Modrow, H. Bonnemann, and C. Kumar, J. Appl. Phys. **97**, 10R102 (2005).
[36] K. Fukumi, A. Chayahara, K. Kadono, H. Kageyama, T. Akai, H. Mizoguchi, N. Kitamura, M. Makihara, Y. Horino, and K. Fujii, J. Mater. Res. **16**, 155 (2001).
[37] J. Shirakawa, M. Nakayama, Y. Uchimoto, and M. Wakihara, Electrochem. Solid-State Lett. **9**, A200 (2006).
[38] C. Song, F. Zeng, Y. X. Shen, K. W. Geng, Y. N. Xie, Z. Y. Wu, and F. Pan, Phys. Rev. B **73**, 172412 (2006).
[39] N. Watanabe, J. Morais, S. B. B. Accione, A. Morrone, J. E. Schmidt, and M. C. M. Alves, J. Phys. Chem. B **108**, 4013 (2004).
[40] L. A. Grunes, Phys. Rev. B **27**, 2111 (1983).
[41] P. Le Fevre, H. Magnan, O. Heckmann, V. Briois, and D. Chandesris, Phys. Rev. B **52**, 11462 (1995).
[42] J. F. Gibbons, Proc. IEEE **60**, 1062 (1972).
[43] R. W. G. Wyckoff, *Crystal Structures* (Interscience, New York, 1963).
[44] H. Dammak, A. Dunlop, and D. Lesueur, Nucl. Instrum. Methods Phys. Res. B **107**, 204 (1996).
[45] H. Trinkaus and A. I. Ryazanov, Phys. Rev. Lett. **74**, 5072 (1995).
[46] P. Kluth, C. S. Schnohr, O. H. Pakarinen, F. Djurabekova, D. J. Sprouster, R. Giulian, M. C. Ridgway, A. P. Byrne, C. Trautmann, D. J. Cookson, K. Nordlund, and M. Toulemonde, Phys. Rev. Lett. **101**, 175503 (2008).
[47] P. Kluth, C. S. Schnohr, D. J. Sprouster, A. P. Byrne, D. J. Cookson, and M. C. Ridgway, Nucl. Instrum. Methods Phys. Res. B **266**, 2994 (2008).
[48] S. Klaumunzer, Nucl. Instrum. Methods Phys. Res. B **225**, 136 (2004).
[49] Z. G. Wang, C. Dufour, E. Paumier, and M. Toulemonde, J. Phys.: Condens. Matter **6**, 6733 (1994).